Analysis of bubble management at different gravity levels by means of an acoustic field

Felix Huber[a], Anna Garcia-Sabaté[a], Dominique Legendre[b], Ricard González-Cinca[a,*]

[a]*Department of Physics, Universitat Politècnica de Catalunya-BarcelonaTech, C/ E. Terradas 5, 08860 Castelldefels, Barcelona (Spain)*
[b]*Institut de Mécanique des Fluides de Toulouse (IMFT), Toulouse (France)*

Abstract

Multiphase flows management is a major challenge in many space applications given the different gravity levels involved. While many of the numerical investigations of liquid-gas phenomena deal with the radial bubble behavior and thus the heat exchange, only a few studies have been conducted on the translational motion of bubbles. We present a numerical investigation of the translational motion of gas bubbles immersed in a liquid that is subject to an acoustic wave at different gravity levels. In the computation, the equations for radial oscillation and translational motion are solved simultaneously. The dynamics of bubbles at different gravity levels (from microgravity to hypergravity) are discussed. Bubbles can be trapped by the acoustic wave at levitation positions in different scenarios. The dependence of the levitation position on the initial bubble position at different pressure amplitudes has been computed, giving rise to the bubble being directed to different nodes of the acoustic wave. The bubble radius also determines if and where the bubble levitates. We propose an analytical criterion for the capture of bubbles in a levitation position in terms of a new dimensionless parameter. The criterion is based on the balance between the average acoustic force and the buoyancy force. With the proposed criterion, the position of bubble levitation can be calculated analytically for any scenario.

Keywords:
2010 MSC: bubble dynamics, acoustics, microgravity, hypergravity, levitation

1. Introduction

The management of multiphase flows is a key aspect in the development of space systems. A better understanding of the behavior of these flows in

*Corresponding author
Email address: ricard.gonzalez@upc.edu (Ricard González-Cinca)

low gravity and hypergravity conditions can enhance the efficiency of different types of systems such as propulsion or life support systems. In propulsion systems, for example, an efficient long-term storage of cryogenic propellants in microgravity environments is a key element to enable new long-range space exploration missions. Cryogenic fluid management in microgravity provides a number of fundamental physical challenges [1, 2, 3, 4]. One of the critical points identified in the different flight phases (propulsive, engine shut-down, ballistic, and preparation of engine restart) is boil-off. Although multi-layer insulation can significantly reduce heat leakage into cryogenic propellant tanks, heat leaks can still take place and become important especially in long-duration mission in liquid hydrogen (with a storage temperature around 20 K), liquid oxygen or methane tanks. Thus, even small heat leakages under microgravity conditions and over long times may give rise to complex large-scale spatiotemporal physical phenomena slowly developing in a multiphase flow. These flows are potentially hazardous in on-orbit operations. An approach based on acoustic waves has been recently proposed to control and eventually eliminate vapour bubbles generated in boil-off [5, 6, 7]. The proposed technique requires far fewer resources than the current used methods (pressurization and thrust), thus being very relevant for cryogenic propellant storage in microgravity. The approach is based on the interaction between bubbles and an external acoustic field.

Bubbles in an acoustic field are under the effects of the primary and secondary Bjerknes forces [8]. The primary Bjerknes force, or acoustic radiation pressure, is the average force exerted on a bubble due to the primary standing acoustic field. The force between two bubbles due to the secondary acoustic field radiated by them is the secondary or mutual Bjerknes force [9]. Most of the studies conducted on the dynamics of bubbles in acoustic fields present analytical models and solutions considering the equations for coupled radial and translational motion of bubbles in weakly compressible liquids [8, 10]. Watanabe and Kukita carried out numerical simulations to investigate the dynamic response of a spherical bubble in a one-dimensional acoustic standing wave field [11]. The authors observed that bubbles larger than the resonance radius move to the node of the pressure field, with small radial oscillations. Bubbles smaller than the resonance radius move to the antinode, featuring larger radial oscillations. Doinikov extended this work by rederiving the equations of motion in translational and radial direction with the Lagrangean formulation [12]. The resulting equations involve an additional term, which provides feedback between the translational motion and the radial bubble pulsations, and couple the equations. The modified radial motion takes the liquid compressibility into account and is suitable for applications in stronger acoustic fields. The interaction between bubbles generated by boiling and an acoustic field has also attracted the interest of researchers. The heat transfer driven by an acoustic standing wave in terrestrial gravity and microgravity was recently investigated [7, 13, 14]. Experiments and numerical simulations to study the bubble motion in a still column of water under an ultrasonic field were carried out at $0g_0$ and $1g_0$, where $g_0 = 9.8m/s^2$ [15]. Measurements of the bubble position and pressure distribution were computed simultaneously to compare theoretical predictions and

experimental observations. The resulting force on the bubble was able to hold it at a stationary position at the node or anti-node of the acoustic field.

We analyze the behavior of bubbles immersed in a liquid under an acoustic field at different gravity levels. Section 2 describes the model used in the study. Section 3 contains the results of the evaluation of two drag models, an analysis of the role played by the acoustic pressure and the bubble radius on the bubble motion, and the analysis of the bubble dynamics at different gravity levels. In Section 4, a criterion for bubble capture or levitation is discussed based on the average acoustic force and the buoyancy force. Conclusions are presented in Section 5.

2. Model

The physical model introduced by Watanabe and Kukita [11], and later used by Abe *et al.* [15], is employed in this study for the calculation of the translational motion of gas bubbles under the influence of an acoustic wave. The model is based on the coupling of the Rayleigh-Plesset equation for the bubble radius with the bubble equation of motion based on the total force acting on the bubbles composed of the force generated by the acoustic radiation pressure, drag force, buoyancy force, and added mass force. The time-averaged translational motion of a bubble is given by the total force acting on it.

$$F_{total} = m_b \frac{du_b}{dt}, \tag{1}$$

where $m_b = \frac{4}{3}\pi R_0^3 \rho_b$ is the mass of the bubble, R_0 and ρ_b being the bubble radius in equilibrium and density, respectively, and $u_b = \frac{\mathrm{d}z}{\mathrm{d}t}$ is the bubble velocity. The equation for the translational motion is coupled with the Rayleigh-Plesset equation, which computes the radial expansion and contraction of the bubble. The numerical code is capable of simulating different gravitational forces and can be varied from microgravity to any hypergravity level.

The effects of the acoustic force on the bubble can be described in terms of the time-averaged translational behavior of the bubbles. In this approach, the acoustic field should be weak, which means that the radial and translational bubble oscillations are required to be sufficiently small [16]. The acoustic radiation pressure acting on the bubble gives rise to the primary and secondary Bjerknes forces [8]. The primary Bjerknes force in its general form can be written as

$$F_{Bj} = -\langle V(t) \nabla P_{ac}(r,t) \rangle, \tag{2}$$

where V is the bubble volume, P_{ac} is the acoustic pressure, r is the radial position, t is time, and $\langle \cdot \rangle$ denotes the average over a cycle. Due to the nonlinear bubble oscillations during the cycle, the average force over a cycle is not zero. An accurate indication of the bubble behavior is given by the Minnaert frequency f_m, which gives the resonance frequency of a gas bubble in a liquid

of density ρ_l:

$$f_m = \frac{1}{\pi d_0}\sqrt{\frac{3\gamma P_{l0}}{\rho_l}}, \tag{3}$$

where $d_0 d$ is the equilibrium bubble diameter, P_{l0} is the hydrostatic pressure of the ambient liquid, and γ is the polytropic index for adiabatic conditions. By rearranging the terms, the Minnaert radius $R_m = d_0/2$ can be obtained. The behavior of bubbles in an acoustic field can be determined by comparing R_m to the initial bubble radius R_0. If $R_0 < R_m$, bubbles will move towards the anti-node of the acoustic field, while if $R_0 > R_m$, bubbles will move to the pressure node. The value of R_m for each study case is presented in the corresponding table in Section 3.

The non-linear oscillations of bubbles in a varying pressure field are described by the Rayleigh-Plesset equation. The derivation of the equation used here considers several assumptions. The bubble is assumed to be in an infinite domain of liquid. Far from the bubble, the liquid is at rest and at a uniform temperature T_∞. The temperature is assumed uniform since there are no heating sources or radiation causing temperature gradients. The liquid pressure far from the bubble, P_∞, is responsible for the regulation of the bubble expansion and reduction in radial direction. Other assumptions are constant liquid density, uniform and constant dynamic viscosity as well as considering a homogeneous content of the bubble. The temperature T_B and pressure P_B within the gas/vapor bubble are always uniform. The generalized Rayleigh-Plesset equation can be written as

$$\frac{P_B(t) - P_\infty(t)}{\rho_l} = R\frac{d^2R}{dt^2} + \frac{3}{2}\left(\frac{dR}{dt}\right)^2 + \frac{4\mu_l}{\rho_l R}\frac{dR}{dt} + \frac{2\sigma}{\rho_l R}, \tag{4}$$

where μ_l is the dynamic viscosity and σ is the surface tension. Eq. 4 can be solved for the radius $R(t)$ when the gas (P_g) and vapor pressure (P_v) inside the bubble $P_B(t)$ are known and the liquid pressure far from the bubble $P_\infty(t)$ is given [17]. Assuming that the process is adiabatic with a polytropic index γ, P_g can be expressed as

$$P_g = P_{g0}\left(\frac{R_0}{R}\right)^{3\gamma}, \tag{5}$$

where P_{g0} is the equilibrium gas pressure in the bubble, which is given by

$$P_{g0} = \frac{2\sigma}{R_0} + P_{l0} - P_v \tag{6}$$

In this study no external heat source is considered, hence P_v can be neglected. The external standing acoustic wave considered here is given by

$$P_{ac} = \Delta P_{ac}\cos(\omega t)\sin(kz), \tag{7}$$

where ΔP_{ac} is the acoustic amplitude, ω the angular frequency and k the wavenumber ($k = 2\pi/\lambda$ with $\lambda = c/f$, where λ is the wavelength and c is the speed of sound in the liquid). Fig. 1 shows the standing acoustic wave in

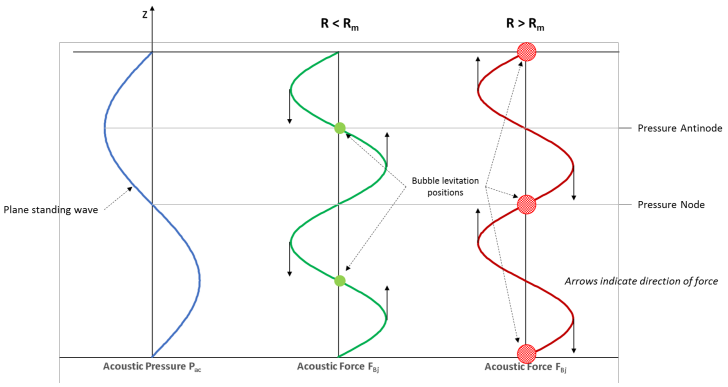

Figure 1: Bubble levitation position in an acoustic wave parallel to gravity.

the direction z parallel to gravity. The bubble levitation position is given for initial bubble radius smaller and larger than the Minnaert radius.

The primary Bjerknes force on a bubble (Eq. 2) generated by the considered acoustic wave is given by

$$F_{Bj} = -V\frac{dP_{ac}}{dz} \tag{8}$$

A bubble in motion in a liquid also experiences a drag force F_D acting against the direction of motion, which is given by

$$F_D = -\frac{1}{2}\rho_l u_r^2 A C_d, \tag{9}$$

where A is the bubble surface, C_d is the drag coefficient for a sphere, and $u_r = u_b - u_l$ is the relative velocity, u_l being the velocity of the liquid given by

$$u_l = -\frac{k\Delta P_{ac}}{\omega\rho_l}\sin(\omega t)\cos(kz) \tag{10}$$

As the bubble moves through the liquid, some volume of the liquid is displaced and accelerated. The associated inertial force on the bubble is known as the added mass force, F_{am}, which is given by

$$F_{am} = \frac{1}{2}\rho_l\frac{d}{dt}(Vu_r) \tag{11}$$

The buoyancy force acting on the bubble is given by

$$F_{buoy} = V(\rho_l - \rho_b)g \tag{12}$$

Hence, the equation for the translational motion of a bubble immersed in a liquid can be expressed as

$$m_b\frac{du_b}{dt} = -V\frac{dP_l}{dz} - \frac{1}{2}\rho_l\frac{d}{dt}(Vu_r) - \frac{1}{2}\rho_l u_r^2 A C_d + V(\rho_l - \rho_b)g, \tag{13}$$

where P_l is the resultant liquid pressure $P_l = P_{l0} + \Delta P_{ac}\cos(\omega t)\sin(kz)$.

A code in FORTRAN was implemented to solve this system of ordinary differential equations composed by the force balance and the Rayleigh-Plesset equations (Eqs. 13 and 4, respectively), by means of the fourth order Runge-Kutta-Gill method.

3. Bubble dynamics

Different scenarios of a single bubble in water have been numerically simulated with variations regarding the bubble interface contamination through its drag model, acoustic pressure, initial radius and gravity level. By changing a series of parameters we are able to compare the results of the simulation with experiments and theoretical predictions. The same boundary conditions apply to all simulations. It is assumed that the bubble motion occurs in an adiabatic system with constant and uniform temperature. Therefore, the generation of the bubble is simply assumed, since there is no internal heat source considered to heat the liquid and generate vapor bubbles. The liquid density is assumed to be constant. The results for the bubble motion are presented in a dimensionless scale, z/λ, showing the bubble motion within one wavelength λ, as well as enabling an evaluation of the bubble movement without the constraints of the specific dimensions of an experimental setup. Table 1 shows the parameters of the liquid (water) and the gas (air) bubble used in the simulations.

Table 1: Liquid and gas parameters.

σ	$7.2 \cdot 10^{-2}$ N/m	ρ_b	1.2 kg/m^3
ρ_l	997.4 kg/m^3	c	1500 m/s
μ_l	$8.9 \cdot 10^{-4}$ Pa·s	γ	1.4
$P_{l0}(= P_\infty)$	100000 Pa		

3.1. Bubble dynamics with an acoustic wave at normal gravity

In this section, the numerical investigation considers a bubble immersed in water and an acoustic wave parallel to gravity. The dynamics of the bubble using two drag models is evaluated. In addition, the impact of the acoustic pressure amplitude and the initial bubble radius on the bubble motion is investigated. An evaluation of the acting forces in this scenario is also carried out.

3.1.1. Drag model analysis

We consider two expressions for the drag coefficient. On the one hand, an expression obtained experimentally by Crum [8], corresponding to contaminated bubbles (*i.e.* bubbles with an immobilized interface):

$$C_d = 27Re^{-0.78}, \tag{14}$$

where Re is the Reynolds number, defined as

$$Re = \frac{2\rho_l u_r R}{\mu_l} \tag{15}$$

Eq. 14 has been experimentally validated for values or Re up to 200 [8]. For this range of Reynolds nuber, Eq. 14 compares well with the Schiller and Naumann [18] drag expression corresponding to solid spheres and usually used for fully contaminated bubbles [19]. On the other hand, we also consider the drag coefficient proposed by Mei *et al.* [20] for clean spherical bubbles (*i.e.* bubbles with a fully mobile interface), which is applicable from zero to infinite Reynolds number:

$$C_d = \frac{16}{Re}\left\{1 + \left[\frac{8}{Re} + \frac{1}{2}(1 + 3.315Re^{-1/2})\right]^{-1}\right\} \tag{16}$$

The parameters used to compute the bubble motion are presented in Table 2. The initial radius of the bubble was varied in the same range as in [15]. Since the other required simulation parameters were not specified by the authors, values from [11] and [21] were used. The initial bubble position was set to $z_0 = z/\lambda = 0.3$, just below a node of the acoustic field at $z/\lambda = 0.5$. The predicted outcome for the simulations is that a bubble could reach an equilibrium position above the node depending of its radius.

Table 2: Parameters for the analysis of the drag models.

$0.51 < R_0 < 1.235$ mm		R_m	0.2237 mm
z_0	0.3	λ	102.88 mm
ΔP_{ac}	20000 Pa	f	14.58 kHz

Fig. 2 shows the bubble motion obtained considering Crum's (Fig. 2a) and Mei's (Fig. 2b) drag models. According to Fig. 2a, only the bubble with the smallest radius can be trapped at a position above the node of the acoustic field. The applied acoustic force is not sufficient to trap the faster rising larger bubbles. If Mei's drag coefficient is considered in the simulations, bubbles rise slightly faster than in the case of Crum's coefficient, and, again, only the smallest bubble can be trapped at the equilibrium position at $z/\lambda = 0.6$, above the node of the acoustic wave. This behavior is qualitatively similar to the observations in [15]. A quantitative comparison with this reference cannot be carried out given the lack of information on all the parameters. The behavior of bubbles does not significantly depend on the employed drag model. In the following simulations, Crum's drag coefficient is used in order to consider fully contaminated bubbles.

3.1.2. Variation of the acoustic pressure amplitude

Table 3 shows the parameters used for the evaluation of the effects of the acoustic pressure amplitude on the bubble motion. Two different bubble initial

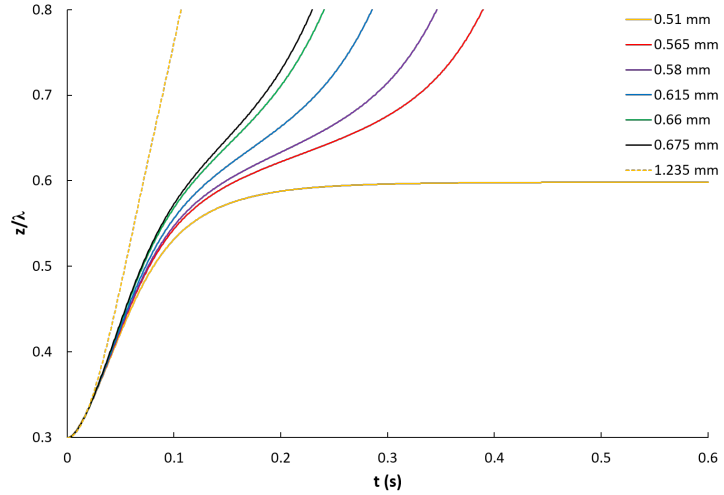

(a)

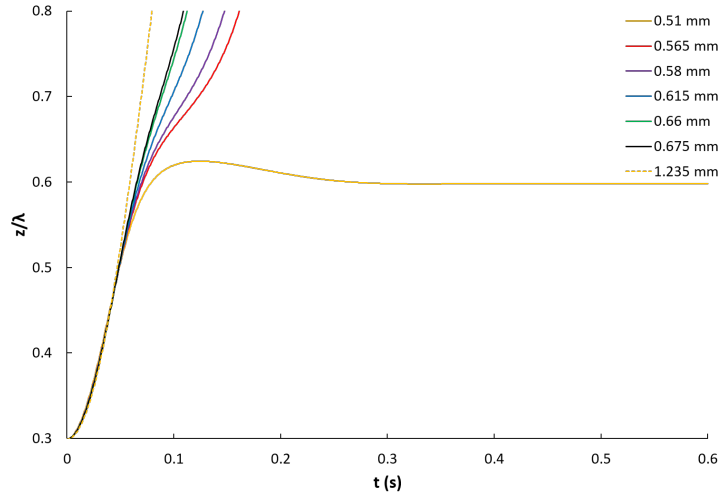

(b)

Figure 2: Bubble motion with different drag models for different bubble diameters: a) Eq. 14, b) Eq. 16.

positions are considered, which, together with the force balance, will determine which node the bubble is moving to.

Fig. 3a shows the behavior of a bubble initially at $z_0 = 0$ for various values of the acoustic pressure amplitude. At low acoustic amplitude ($\Delta P_{ac} \leq 40$ kPa), the buoyancy force overcomes the acoustic force and pushes the bubble upwards. At $\Delta P_{ac} = 45$ kPa, the buoyancy force is compensated by the acoustic force and the bubble remains in levitation above the node of the acoustic wave at $z/\lambda = 0$.

Table 3: Parameters for the analysis of the variation of the acoustic pressure amplitude.

R_0	0.5 mm	R_m	0.05436 mm
z_0	0 and 0.2	λ	25 mm
$1 < \Delta P_{ac} < 100$ kPa		f	60 kHz

As the acoustic pressure increases, the bubble barely rises and stabilizes faster at a lower position.

When the initial position of the bubble is set to $z_0 = 0.2$, an acoustic pressure amplitude of at least 45 kPa is needed to overcome the buoyancy force and trap the bubble above the node at $z/\lambda = 0.5$ (Fig. 3b). The bubble takes approximately 0.15 seconds to reach an equilibrium position. Bubbles under a lower acoustic pressure rise and escape the pressure node. The bubble motion for more than one wavelength at $\Delta P_{ac} < 45$ kPa consists on the rising bubble slowing down towards a pressure node, and accelerating after crossing it. As the pressure increases, the bubble rises more slowly. At $P_{ac} \geq 60$ kPa the acoustic force pushes the bubble downwards to the node at $z/\lambda = 0$. Furthermore, the time needed to reach the position of levitation is reduced to 0.1 seconds. For the highest acoustic amplitude applied, simulations show that the bubble is pushed even below the node at $z/\lambda = 0$ before reaching a levitation position just above it. It should be noted the overlapping of lines corresponding to the lowest pressure amplitudes (namely 1, 2 and 5 kPa) in Figs. 3a and 3b. The acoustic effects in these cases are so weak that bubbles rise towards the free surface following a very similar trajectory.

The results in Figs. 3a and 3b show that a bubble can be captured by an acoustic wave provided its amplitude is sufficiently high, as observed in experiments in [21]. Figs. 4a and 4b show the levitation position for different acoustic amplitudes obtained from the model solution (dots) with starting positions at $z_0 = 0$ and $z_0 = 0.2$, respectively. The position of bubble capture is significantly impacted by the acoustic pressure amplitude. Lines correspond to the theoretical prediction of the levitation position, which can be obtained from the average acoustic force on a bubble propagating in the z-direction obtained from Eqs. 7 and 8 [13]:

$$F_{avg} = \frac{2\pi^2 R_0^3 \Delta P_{ac}^2}{3P_{l0}\gamma\lambda(1-\frac{\omega^2}{\omega_m^2})} sin(4\pi\frac{z}{\lambda}), \tag{17}$$

where $\omega_m = 2\pi f_m$. A bubble levitation position is reached when the average acoustic force (Eq. 17) and the buoyancy force (Eq. 12) become equal. The dimensionless levitation position z/λ can be obtained by rearranging the terms of the force balance equation. This capture criterion is discussed in more detail in Section 4. Figs. 4a and 4b show that the numerical results are in good agreement with the capture criterion.

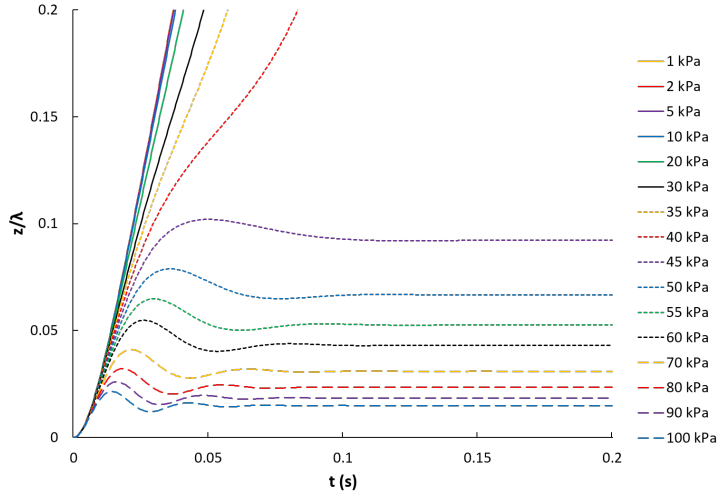

(a)

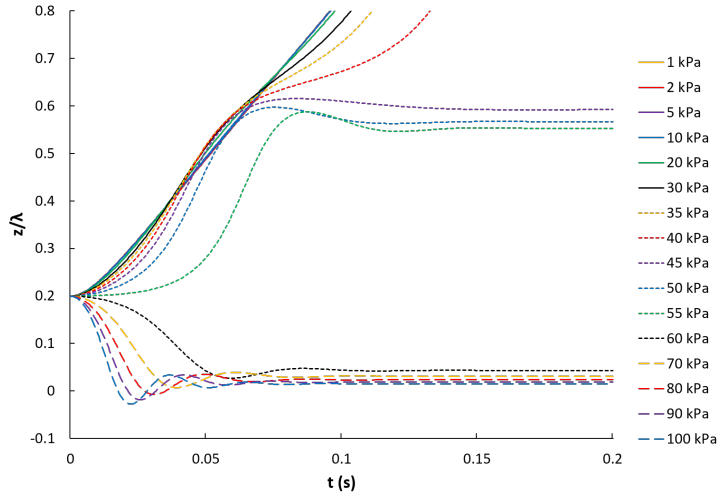

(b)

Figure 3: Bubble motion at different acoustic pressure amplitudes and starting positions: a) $z_0 = 0$, b) $z_0 = 0.2$.

3.1.3. Variation of the initial bubble radius

Table 4 shows the set of parameters used for the simulation of the bubble motion with different initial bubble radii.

Fig. 5 shows the bubble motion for different initial radii. Larger bubbles rise faster thanks to a higher buoyancy force and can avoid acoustic trapping. As the radius is decreased, buoyancy can be compensated by the acoustic radiation pressure, reaching a levitation position above the node at $z/\lambda = 0.5$. For the

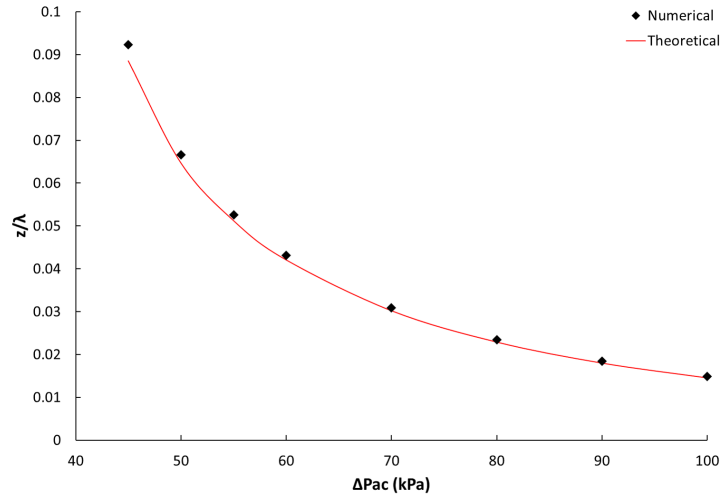

(a)

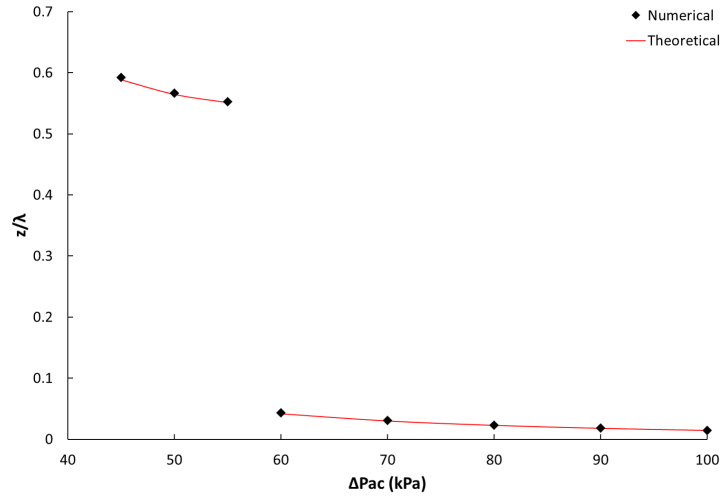

(b)

Figure 4: Levitation position at different acoustic pressure amplitudes and starting positions. Dots: model, lines: Eq. 18. a) $z_0 = 0$, b) $z_0 = 0.2$.

smallest bubbles the buoyancy force is overcome by the acoustic force, which pushes them down towards the node at $z/\lambda = 0$. Moreover, the time needed to reach levitation is reduced as the bubble size is decreased.

Fig. 6 shows the levitation position for different initial bubble radii obtained from the numerical simulations (dots) and the theoretical prediction of the levitation position discussed in Section 4 (lines). Again, the numerical results are in good agreement with the capture criterion considered in the analytical

Table 4: Parameters for the analysis of the variation of the initial radius.

$0.385 < R_0 < 1.019$ mm		R_m	0.05436 mm
z_0	0.2	λ	25 mm
ΔP_{ac}	50000 Pa	f	60 kHz

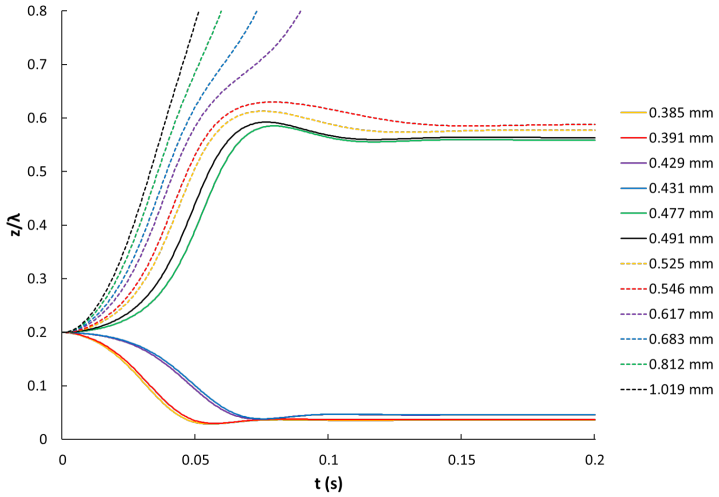

Figure 5: Bubble motion for different initial radii.

prediction.

3.1.4. Evaluation of forces

The set of parameters used for the evaluation of the forces acting on a bubble (Table 5) are the same as in [15].

Table 5: Parameters for the evaluation of forces.

R_0	0.5 mm	R_m	0.1664 mm
z_0	0.3	λ	76.53 mm
ΔP_{ac}	60000 Pa	f	19.6 kHz

Fig. 7 shows the time evolution of the forces acting on the bubble for a short period (24.5 ms $< t <$ 24.7 ms) during the initial rise of the bubble. Given the difference in the order of magnitude of the forces, they are plotted separately. Both Figs. 7a and 7b have the same scale in the horizontal axis to ease a direct comparison.

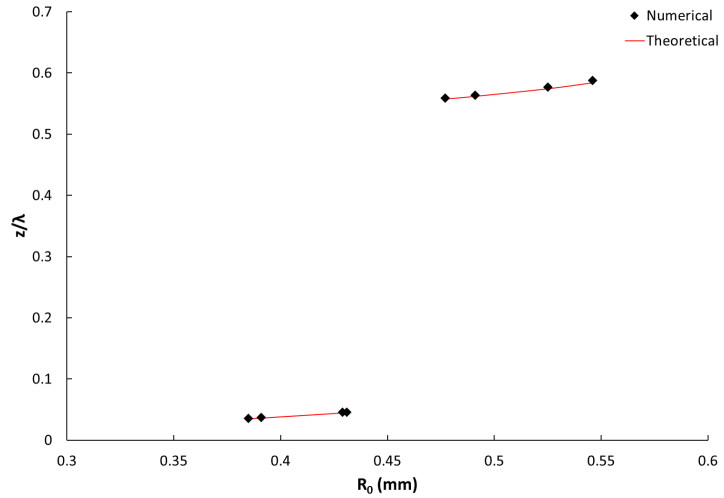

Figure 6: Levitation position for different bubble radii. Dots: model, lines: Eq. 18.

Fig. 7a shows the total, drag, and buoyancy force, of magnitude $10^{-5}N$. The small size of the considered bubble gives rise to a drag force with a little impact in the total force and translational motion of the bubble. However, the buoyancy force plays an important role in the total force, as the acoustic and added mass force do (Fig. 7b). The primary Bjerknes force is in phase with the total force, while the added mass force is shifted $\pi/2$. The results in Figs. 7a and 7b are consistent with [15], which confirms the validity of the numerical procedure employed in this study.

3.2. Bubble dynamics with an acoustic wave at different gravity levels

In this section, the effect of the gravity level on the dynamics of the bubble is examined. The behavior of the bubble velocity and trajectory at low gravity and hypergravity levels is analyzed. An evaluation of the acting forces in this scenario is also carried out.

Table 6 shows the set of parameters used for the simulations of the bubble behavior at different gravity levels. The acoustic pressure amplitude is changed to evaluate the required acoustic field to trap the bubble in an equilibrium position at different gravitational environments.

Table 6: Parameters for the analysis of the gravity level variation.

R_0	0.5 mm	R_m	0.1664 mm
z_0	0.45	λ	76.53 mm
ΔP_{ac}	60000 Pa	f	19.6 kHz
	280000 Pa		

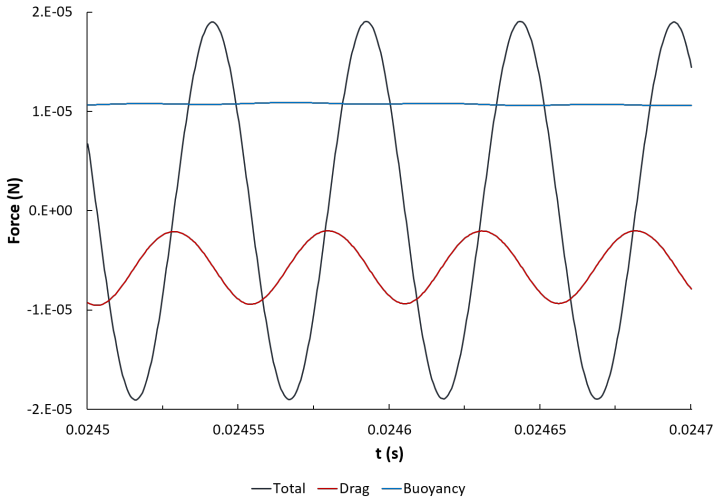

(a)

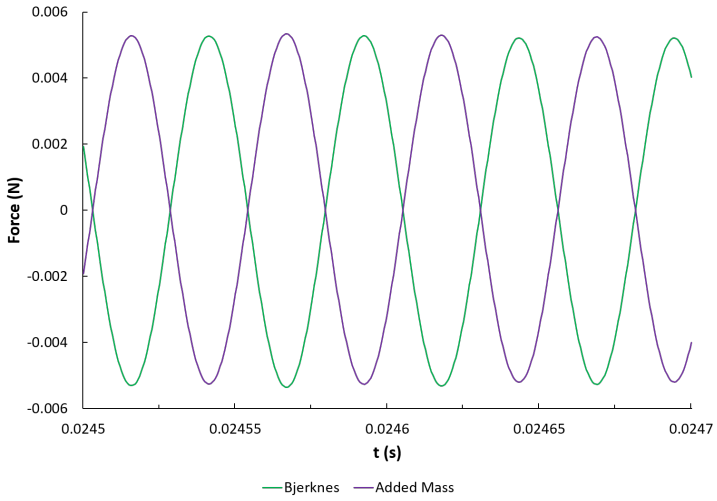

(b)

Figure 7: Time evolution of forces: a) Total, drag, and buoyancy, b) Acoustic and added mass.

3.2.1. Bubble velocity

Fig. 8 shows the bubble velocity as a function of time at a gravity level of $2g_0$ for two different acoustic pressure amplitudes. The black line corresponds to an acoustic amplitude sufficiently large to keep the bubble trapped in an equilibrium position. After an initial velocity peak, the bubble slows down and the velocity tends to zero, which indicates that the bubble remains at a position near the pressure node of the acoustic field. The red dashed line shows the

bubble velocity for a slightly reduced acoustic pressure amplitude. In this case, the bubble cannot be trapped by the acoustic force and moves towards the free surface. Every time the bubble approaches a pressure node, the bubble is slowed down. After passing a node, the bubble velocity increases towards the antinode of the pressure field, and is subsequently decelerated when approaching the next pressure node.

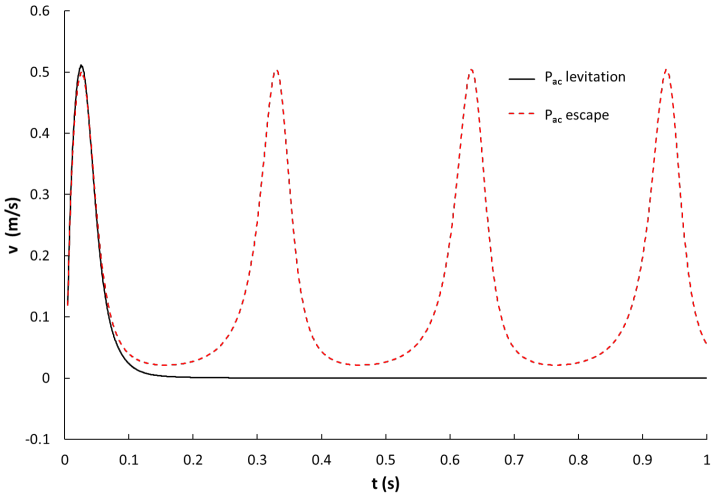

Figure 8: Bubble velocity for acoustic pressure amplitudes at $2g_0$.

Figs. 9a and 9b show the bubble velocity as a function of time at low gravity and hypergravity levels, respectively. The pressure amplitude for the simulations was set to the minimum required pressure needed to trap the bubble. The bubble velocity at low gravity is lower than at hypergravity levels, which makes the bubble to need longer times to reach the pressure node as gravity decreases. The velocity peak at hypergravity is significantly higher than at reduced gravity. In all the presented cases, the bubble slowed down approaching a pressure node and finally stabilized at it.

3.2.2. Bubble trajectory

The bubble trajectory at low and hypergravity levels is analyzed. Simulations for bubbles at low gravity levels were carried out with an acoustic pressure amplitude of 60 kPa, which is 2.5 times higher than the required acoustic amplitude to trap a bubble at $1g_0$. At hypergravity levels, ΔP_{ac} was set to 280 kPa to ensure that all bubbles were trapped at the node.

Figs. 10a and 10b show the bubble motion at low gravity and hypergravity levels, respectively. In all cases, the bubble rises above the levitation position (higher as the gravity level increases) and oscillates around it before stabilizing. The number of oscillations and the time for stabilization are related to the applied acoustic amplitude. In the case of $1g_0$, for instance, the bubble performs

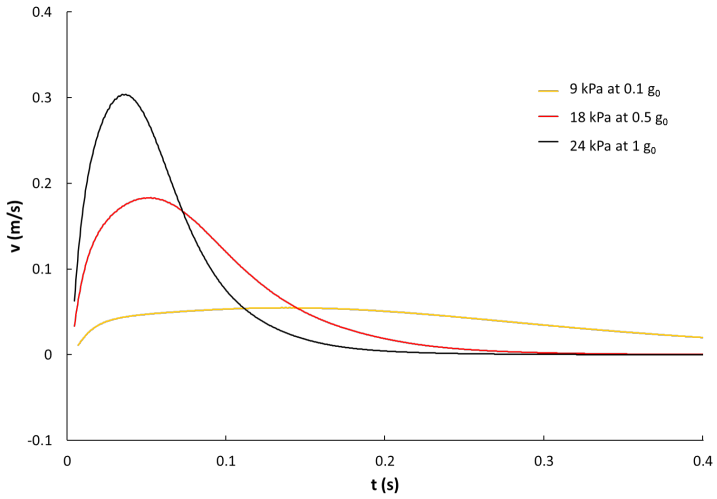

(a)

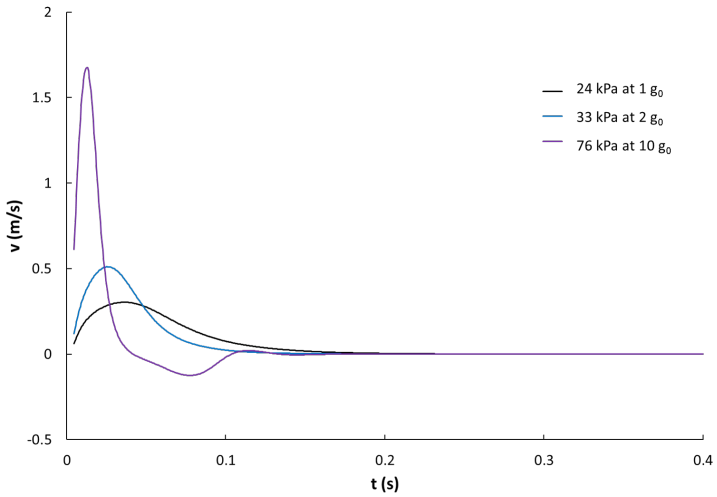

(b)

Figure 9: Bubble velocity at different gravity levels: a) Low gravity, b) Hypergravity.

fewer oscillations of larger period and requires a longer time to stabilize at lower pressure amplitude (Fig. 10a).

Figs. 11a and 11b show the levitation position of bubbles at low gravity and hypergravity levels, respectively, obtained from the numerical simulations (dots) and the theoretical prediction of the levitation position discussed in Section 4 (lines). The numerical results are in good agreement with the capture criterion considered in the analytical prediction. In both low gravity and hypergravity cases, if ΔP_{ac} is constant, the levitation position of the bubbles features a linear

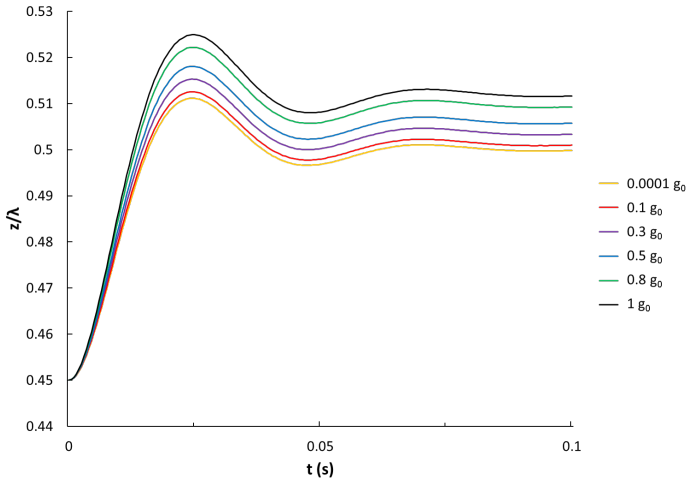

(a)

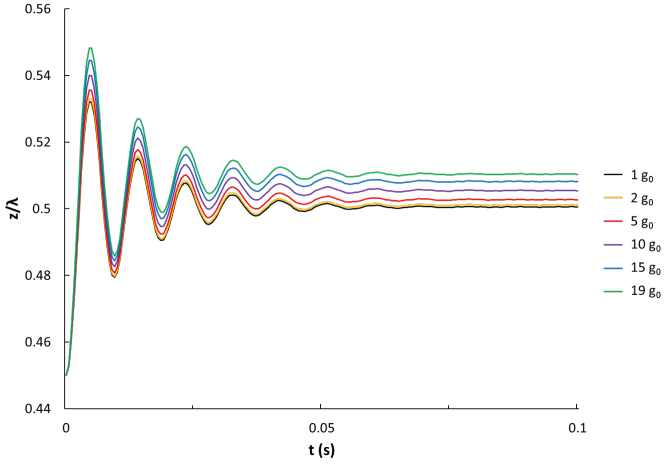

(b)

Figure 10: Bubble motion at different gravity levels: a) Low gravity with $\Delta P_{ac} = 60$ kPa, b) Hypergravity with $\Delta P_{ac} = 280$ kPa.

dependency with the gravity level.

Figs. 12a and 12b show the required acoustic pressure amplitude to keep the bubble in a levitation position at low gravity and hypergravity levels, respectively. Dots correspond to the model computed values and lines to second degree polynomial fittings. The required acoustic amplitude for bubble levitation grows with gravity level only slightly faster at hypergravity than at low gravity.

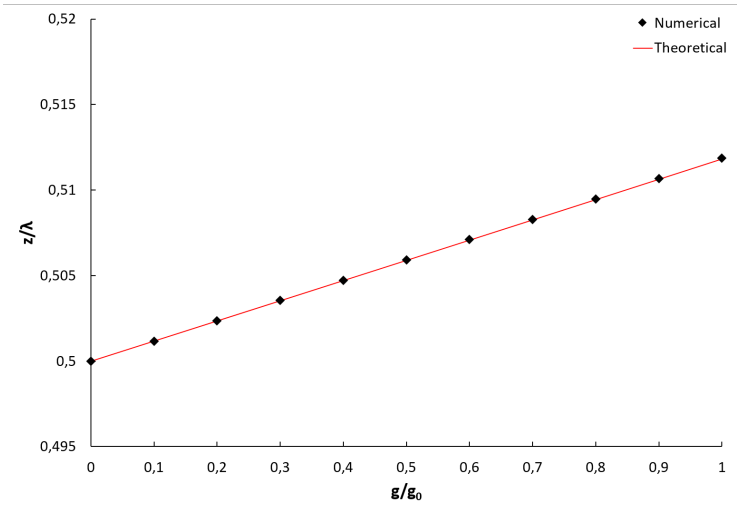

(a)

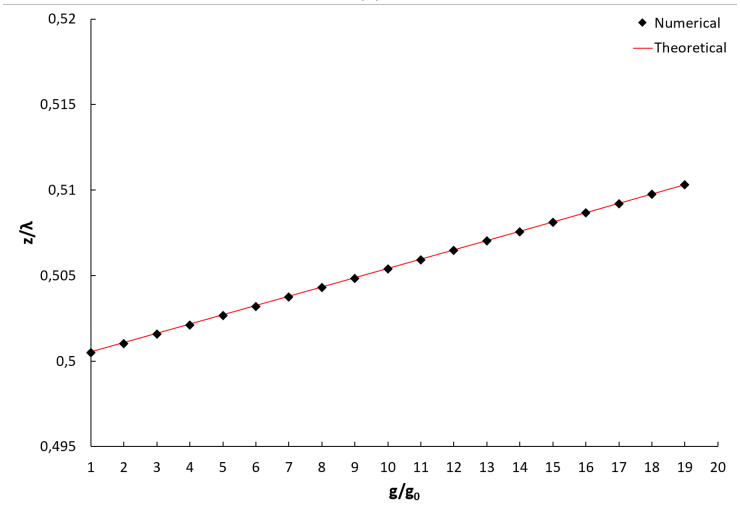

(b)

Figure 11: Levitation position at different gravity levels. Dots: model, lines: Eq. 18. a) Low gravity with $\Delta P_{ac} = 60$ kPa, b) Hypergravity with $\Delta P_{ac} = 280$ kPa.

3.2.3. Evaluation of forces

Table 7 shows the maximum value of all the forces acting on a bubble of radius 0.5 mm when the acoustic pressure amplitude is sufficiently large to keep the bubble levitating at the node. Table 8 shows the value of all the forces acting on a bubble that escapes the pressure node. Note that the Bjerknes force must be increased at growing gravity level in order to trap the bubble in a levitation position. However, the largest variation in magnitude as the gravity level is

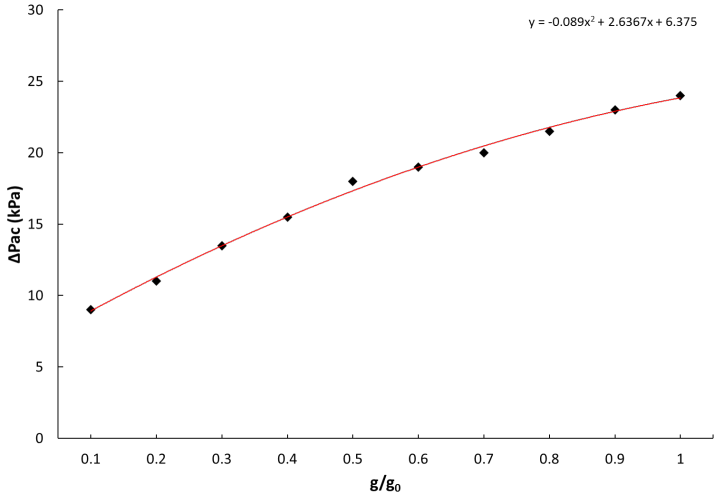

(a)

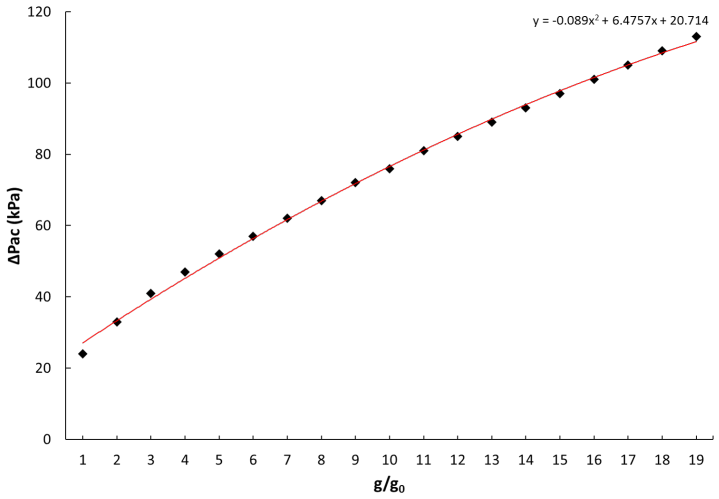

(b)

Figure 12: Acoustic pressure amplitude required for bubble levitation at different gravity levels. Dots: model, lines: fit. a) Low gravity, b) Hypergravity.

changed corresponds to the buoyancy force.

4. Condition for bubble capture

The bubble levitation position can be predicted by equalising the average acoustic force (Eq. 17) and the buoyancy force (Eq. 12). This bubble capture criterion gives rise to two possible dimensionless bubble levitation positions in

Table 7: Forces for bubble levitation at different gravity levels.

g	F_{total}	F_D	F_{buoy}	F_{bj}	F_{am}
$0.0001g_0$	$4.07 \cdot 10^{-7}$	$3.08 \cdot 10^{-7}$	$5.11 \cdot 10^{-10}$	$1.13 \cdot 10^{-4}$	$1.12 \cdot 10^{-4}$
$0.1g_0$	$5.03 \cdot 10^{-7}$	$8.93 \cdot 10^{-7}$	$5.11 \cdot 10^{-7}$	$1.39 \cdot 10^{-4}$	$1.38 \cdot 10^{-4}$
$0.3g_0$	$9.18 \cdot 10^{-7}$	$2.59 \cdot 10^{-6}$	$1.53 \cdot 10^{-6}$	$2.50 \cdot 10^{-4}$	$2.48 \cdot 10^{-4}$
$0.5g_0$	$1.45 \cdot 10^{-6}$	$4.75 \cdot 10^{-6}$	$2.55 \cdot 10^{-6}$	$3.93 \cdot 10^{-4}$	$3.88 \cdot 10^{-4}$
$0.8g_0$	$2.04 \cdot 10^{-6}$	$7.61 \cdot 10^{-6}$	$4.08 \cdot 10^{-6}$	$5.50 \cdot 10^{-4}$	$5.43 \cdot 10^{-4}$
$1g_0$	$2.52 \cdot 10^{-6}$	$9.77 \cdot 10^{-6}$	$5.10 \cdot 10^{-6}$	$6.73 \cdot 10^{-4}$	$6.65 \cdot 10^{-4}$
$2g_0$	$4.66 \cdot 10^{-6}$	$1.95 \cdot 10^{-5}$	$1.02 \cdot 10^{-5}$	$1.23 \cdot 10^{-3}$	$1.22 \cdot 10^{-3}$
$5g_0$	$7.88 \cdot 10^{-6}$	$2.57 \cdot 10^{-5}$	$2.55 \cdot 10^{-5}$	$2.10 \cdot 10^{-3}$	$2.15 \cdot 10^{-3}$
$10g_0$	$8.29 \cdot 10^{-6}$	$9.16 \cdot 10^{-6}$	$5.07 \cdot 10^{-5}$	$2.15 \cdot 10^{-3}$	$2.28 \cdot 10^{-3}$
$15g_0$	$8.14 \cdot 10^{-6}$	$2.47 \cdot 10^{-6}$	$7.65 \cdot 10^{-5}$	$2.14 \cdot 10^{-3}$	$2.42 \cdot 10^{-3}$
$19g_0$	$8.55 \cdot 10^{-6}$	$1.22 \cdot 10^{-7}$	$9.87 \cdot 10^{-5}$	$2.31 \cdot 10^{-3}$	$2.51 \cdot 10^{-3}$

Table 8: Forces for bubble escape at different gravity levels.

g	F_{total}	F_D	F_{buoy}	F_{bj}	F_{am}
$0.0001g_0$	$2.97 \cdot 10^{-7}$	$-1.70 \cdot 10^{-7}$	$5.24 \cdot 10^{-10}$	$8.25 \cdot 10^{-5}$	$8.22 \cdot 10^{-5}$
$0.1g_0$	$3.81 \cdot 10^{-7}$	$-7.29 \cdot 10^{-7}$	$5.24 \cdot 10^{-7}$	$1.05 \cdot 10^{-4}$	$1.05 \cdot 10^{-4}$
$0.3g_0$	$7.19 \cdot 10^{-7}$	$-2.23 \cdot 10^{-6}$	$1.57 \cdot 10^{-6}$	$1.96 \cdot 10^{-4}$	$1.95 \cdot 10^{-4}$
$0.5g_0$	$1.25 \cdot 10^{-6}$	$-4.33 \cdot 10^{-6}$	$2.62 \cdot 10^{-6}$	$3.37 \cdot 10^{-4}$	$3.34 \cdot 10^{-4}$
$0.8g_0$	$1.85 \cdot 10^{-6}$	$-7.26 \cdot 10^{-6}$	$4.19 \cdot 10^{-6}$	$4.99 \cdot 10^{-4}$	$4.93 \cdot 10^{-4}$
$1g_0$	$2.23 \cdot 10^{-6}$	$-9.18 \cdot 10^{-6}$	$5.23 \cdot 10^{-6}$	$5.98 \cdot 10^{-4}$	$5.92 \cdot 10^{-4}$
$2g_0$	$4.28 \cdot 10^{-6}$	$-1.90 \cdot 10^{-5}$	$1.05 \cdot 10^{-5}$	$1.13 \cdot 10^{-3}$	$1.12 \cdot 10^{-3}$
$5g_0$	$7.62 \cdot 10^{-6}$	$-2.76 \cdot 10^{-5}$	$2.61 \cdot 10^{-5}$	$2.03 \cdot 10^{-3}$	$2.08 \cdot 10^{-3}$
$10g_0$	$8.14 \cdot 10^{-6}$	$-1.20 \cdot 10^{-5}$	$5.19 \cdot 10^{-5}$	$2.07 \cdot 10^{-3}$	$2.19 \cdot 10^{-3}$
$15g_0$	$7.63 \cdot 10^{-6}$	$-6.61 \cdot 10^{-6}$	$7.81 \cdot 10^{-5}$	$1.93 \cdot 10^{-3}$	$2.17 \cdot 10^{-3}$
$19g_0$	$7.76 \cdot 10^{-6}$	$-7.66 \cdot 10^{-6}$	$1.01 \cdot 10^{-4}$	$1.85 \cdot 10^{-3}$	$2.01 \cdot 10^{-3}$

a given wavelength λ:

$$\frac{z_1}{\lambda} = \frac{1}{4\pi} \arcsin\left(\frac{1}{6\pi}\left(\frac{\rho_l g d_0}{\Delta P_{ac}}\right)^2 \frac{\lambda(\omega_m^2 - \omega^2)}{g}\right) \tag{18}$$

$$\frac{z_2}{\lambda} = \frac{1}{2} + \frac{1}{4\pi} \arcsin\left(\frac{1}{6\pi}\left(\frac{\rho_l g d_0}{\Delta P_{ac}}\right)^2 \frac{\lambda(\omega_m^2 - \omega^2)}{g}\right) \tag{19}$$

Therefore, the capture position is controlled by the parameter $\mathcal{C} = g\rho_l^2 d_0^2 \lambda(\omega_m^2 - \omega^2)/6\pi\Delta P_{ac}^2$. $\mathcal{C}$ can be decomposed as the product of the normalized oscillation $\lambda(\omega_m^2 - \omega^2)/6\pi g$ and the square of the parameter $\mathcal{P} = \rho_l g d_0/\Delta P_{ac}$, that compares the hydrostatic pressure at the bubble scale $\rho_l g d_0$ to the acoustic pressure ΔP_{ac}.

Fig. 13 shows the bubble levitation position as a function of $\mid \mathcal{C} \mid$. Symbols correspond to the simulations reported above (with varying pressure amplitude,

bubble radius, and gravity level). Lines correspond to capture positions given by Eqs. 18 and 19. The capture position corresponding to Eq. 19 is shifted 0.5 in the vertical axis so that the two positions of capture depending on the starting position of the bubble, z_0, are reproduced. All the data collapse on Eqs. 18 and 19, that are able to predict the capture position for any practical condition. In addition, a capture criterion can be proposed. A capture is possible if the followng condition on $\mathcal{C}$ is satisfied

$$-1 \leq \mathcal{C} = \frac{g\rho_l^2 d_0^2 \lambda(\omega_m^2 - \omega^2)}{6\pi\Delta P_{ac}^2} \leq 1 \tag{20}$$

The previous simulations for captured and not captured bubbles are reported in Fig. 14, where a phase diagram showing $\mid \mathcal{C} \mid$ as a function of $\mathcal{P}$ is proposed. Experimental points obtained from [13] are included in the figure. In these experiments, bubbles of 0.99 mm radius in FC-72 at normal gravity conditions with an acoustic pressure amplitude varying between 28 and 70 kPa are considered. All the simulations and the Moehrle *et al.* points in the capture and non-capture sides of the phase diagram correspond to scenarios of bubble capture and non-capture, respectively. Additional experimental points obtained from data in [15] are also included in the figure. Authors considered in their experiments and simulations air bubbles in water with a diameter ranging between 1.02 mm and 2.47 mm at normal gravity conditions with an acoustic pressure amplitude of 0.02 MPa. If one assumes the reported value to correspond to 20 kPa, two points in the phase diagram corresponding to a capture case would be above the $C = 1$ line. However, if one considers the acoustic amplitude to be 23 kPa, there is a total matching between the capture criterion and the experimental observations (Fig. 14). We can conclude that both our simulations and the experimental results from [13, 15] match perfectly with the proposed phase diagram for the capture criterion.

5. Conclusions

Several space systems (such as those for propulsion or life support) require an accurate management of multiphase flows at different gravity levels. The possibility to control the position of a bubble in a liquid is important for many processes involving multiphase flows. The use of acoustic waves is a promising approach for bubble management. Most of the research on bubbles in an acoustic wave has been focussed up until now on the radial bubble oscillations and the involved thermodynamic processes. We have carried out an investigation on the behavior of bubbles in an acoustic wave parallel to gravity at different gravity levels (low gravity and hypergravity) with a focus on the bubble translational motion. A physical model based on the force balance and the Rayleigh-Plesset equation has been solved by means of the Runge-Kutta-Gill approach to determine the bubble dynamics. The analysis of the bubble dynamics at different pressure amplitudes showed the dependence of the levitation position on the initial bubble position at different pressure amplitudes, which gave rise to the

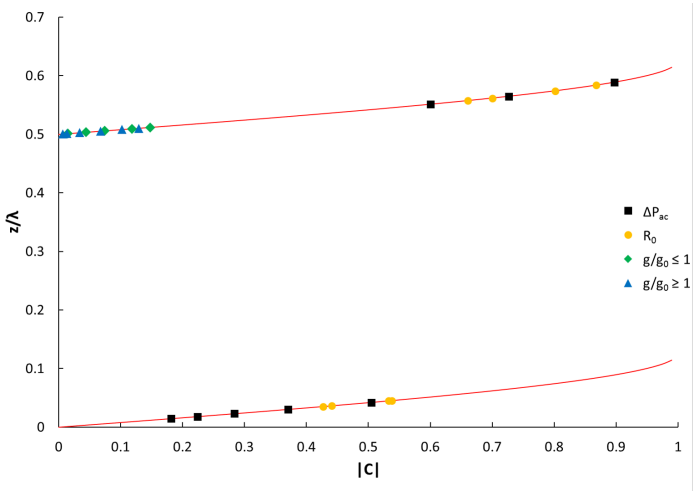

Figure 13: Bubble levitation position as a function of the parameter $\mathcal{C}$. Symbols: simulations. Lines: Eq. 18 and Eq. 19 for capture position z_1 and z_2, respectively.

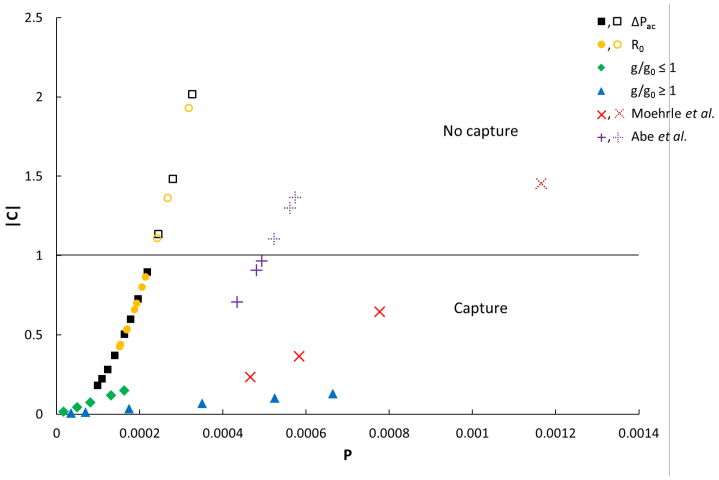

Figure 14: Phase diagram for the capture condition. Symbols: simulations for the different cases considered with varying pressure amplitude, bubble radius, and gravity level, and experiments in [13, 15]. Filled symbols correspond to capture, outlined/dashed symbols correspond to non-capture. Line: capture criterion from Eq. 20.

bubble being directed to the upper or to the lower node. The bubble levitation on either node depends also on its radius. The behavior of bubbles in an acoustic wave at different gravity levels (from $0g_0$ to $19g_0$) has also been studied by means of the analysis of the bubble trajectory and velocity, and the magnitude of the forces. We have proposed a capture criterion based on the balance between the average acoustic force and the buoyancy force. We can

confirm that the levitation position at different acoustic pressure amplitude, radius and gravity level can be determined with the proposed criterion. This was validated by numerical and analytical evaluation and compared with published experimental data. Further experimental validation of our capture criterion can be carried out in microgravity platforms, parabolic flights providing Moon and Mars gravity levels, and centrifuges providing hypergravity levels.

6. Acknowledgements

This research was funded by the Agencia Estatal de Investigación (Spain) project ESP2016-79196-P (AEI/FEDER, UE).

References

[1] S. M. Motil, M. L. Meyer, S. P. Tucker, Cryogenic fluid management technologies for advanced green propulsion systems, Technical Report TM-2007-214810, NASA (2007).

[2] D. J. Chato, Low gravity issues of cryogenic fluid management technologies enabling exploration, National Academies, 2009.

[3] M. P. Doherty, J. D. Gaby, L. J. Salerno, S. G. Suttherlin, Cryogenic fluid management technology for moon and mars missions, Technical Report TM-2010-216070, NASA (2010).

[4] C. B. Muratov, V. N. Smelyanskiy, R. W. Tyson, Nucleate boiling in long-term cryogenic propellant storage in microgravity, 62nd International Astronautical Congress (South Africa), IAC-11, A2.6.4.x12034 (2011).

[5] G. Quintana-Buil, A. Garcia-Sabaté, S. Batlle, G. López, V. Sierra, O. Casas, R. González-Cinca, A sounding rocket experiment to control boiling by means of acoustic waves, Microgravity Science and Technology 29(5) (2018) 731–736.

[6] F. Suñol, D. A. Ochoa, M. Granados, R. González-Cinca, J. E. García, Performance assessment of ultrasonic waves for bubble control in cryogenic fuel tanks, Microgravity Science and Technology 32 (2020) 609–613. doi:https://doi.org/10.1007/s12217-020-09795-y.

[7] G. Quintana-Buil, R. González-Cinca, Acoustic effects on heat transfer on the ground and in microgravity conditions, Submitted to International Journal of Heat and Mass Transfer (2020).

[8] L. A. Crum, Bjerknes forces on bubbles in a stationary sound field, The Journal of the Acoustical Society of America 57 (6) (1975) 1363. doi:10.1121/1.380614.

[9] A. Garcia-Sabaté, A. Castro, M. Hoyos, R. González-Cinca, Experimental study on inter-particle acoustic forces, J. Acoust. Soc. Am. 135(3) (2014) 1056–1063.

[10] A. A. Doinikov, Equations of coupled radial and translational motions of a bubble in a weakly compressible liquid, Physics of Fluids 17 (12) (2005) 1–4. doi:10.1063/1.2145430.

[11] T. Watanabe, Y. Kukita, Translational and radial motions of a bubble in an acoustic standing wave field, Physics of Fluids A 5 (11) (1993) 2682–2688. doi:http://dx.doi.org/10.1063/1.858731.

[12] A. A. Doinikov, Translational motion of a spherical bubble in an acoustic standing wave of high intensity, Physics of Fluids 14 (4) (2002) 1420–1425. doi:10.1063/1.1458597.

[13] R. E. Moehrle, J. N. Chung, Pool boiling heat transfer driven by an acoustic standing wave in terrestrial gravity and microgravity, International Journal of Heat and Mass Transfer 93 (2016) 322–336. doi:10.1016/j.ijheatmasstransfer.2015.09.030.

[14] L. Wang, K. Zhu, F. Xie, Y. Ma, Y. Li, Prediction of pool boiling heat transfer for hydrogen in microgravity, International Journal of Heat and Mass Transfer 94 (2016) 465–473. doi:10.1016/j.ijheatmasstransfer.2015.11.049.

[15] Y. Abe, M. Kawaji, T. Watanabe, Study on the bubble motion control by ultrasonic wave, Experimental Thermal and Fluid Science 26 (6-7) (2002) 817–826. doi:10.1016/S0894-1777(02)00197-8.

[16] A. A. Doinikov, Bjerknes forces and translational bubble dynamics, Bubble and particle dynamics in acoustic fields: modern trends and applications 661 (2005) 95–143.

[17] C. E. Brennen, Cavitation and bubble dynamics, Oxford University Press, 1995.

[18] V. L. Schiller, A. Z. Naumann, Uber die grundlegende Berechnung bei der Schwerkraftaufbereitung, Ver. Deut. Ing. Zeitung 77 (1933) 318–320.

[19] A. Tomiyama, I. Kataoka, I. Zun, T. Sakaguchi, Drag coefficients of single bubbles under normal and micro gravity conditions, JSME International journal 41(2) (1998) 472–479.

[20] R. Mei, J. F. Klausner, C. J. Lawrence, A note on the history force on a spherical bubble at finite Reynolds number, Physics of Fluids 6 (1) (1994) 418–420. doi:10.1063/1.868039.

[21] A. Garcia-Sabaté, Effects of Vibrations Applied To Fluids at Different Gravity Levels, Ph.D. thesis, Universitat Politècnica de Catalunya (2016).